Balanced Response of an Axisymmetric Tropical Cyclone to Periodic Diurnal Heating

ERIKA L. NAVARRO[a] AND GREGORY J. HAKIM

Department of Atmospheric Sciences, University of Washington, Seattle, Washington

HUGH E. WILLOUGHBY

Department of Earth and Environment, Florida International University, Miami, Florida

ABSTRACT

A modified version of the Sawyer–Eliassen equation is applied to determine the impact of periodic diurnal heating on a balanced vortex. The TC diurnal cycle is a coherent signal that arises in the cirrus canopy. However, despite thorough documentation in the literature, the dynamical mechanism remains unknown. Recent work demonstrates that periodic radiative heating in the TC outflow layer is linked with an anomalous upper-level circulation; this heating is also associated with a cycle of latent heating in the lower troposphere that corresponds to a cycle in storm intensity. Using a method that is analogous to the Sawyer–Eliassen equation, but for solutions having the same time scale as time-periodic forcing, these distributions are analyzed to determine the effect of periodic diurnal heating on an axisymmetric vortex.

Results for periodic heating in the lower troposphere show an overturning circulation that resembles the Sawyer–Eliassen solution. The model simulates positive perturbations in the azimuthal wind field of $2.5\,\mathrm{m\,s}^{-1}$ near the radius of maximum wind. Periodic heating near the top of the vortex produces a local overturning response in the region of heating and an inertia–buoyancy wave response in the storm environment. Comparison of the results from the modified Sawyer–Eliassen equation to those of an idealized axisymmetric solution for both heating distributions shows similarities in the structure of the perturbation wind fields, suggesting that the axisymmetric TC diurnal cycle is primarily a balanced response driven by periodic heating.

1. Introduction

Recent observations demonstrate a clear diurnal signal in the high clouds of tropical cyclones (TCs). However, although this oscillation is linked to storm structure and intensity, the impact of periodic diurnal heating in TCs is not well understood. A numerical study examining the TC diurnal cycle in a statistically steady-state framework shows a periodic wind and temperature response (Navarro and Hakim 2016, hereafter NH2016): periodic heating in the TC outflow layer from the daily cycle of radiation coincides with a local overturning circulation,

with inflow toward the base of the heating, upward motion in the region of heating, and radial outflow at the top of the heat source. Inertia–buoyancy waves are observed in the upper troposphere and lower stratosphere, mainly in the periodic temperature response. A second periodic signal is observed in the lower troposphere, where a diurnal oscillation in the latent heating tendency field leads a periodic response in the azimuthal wind by approximately 6 h. NH2016 propose that the dynamic response to periodic heating drives a circulation in these two regions that produces the diurnal cycle in the TC wind field. Here, we use a modified Sawyer–Eliassen approach for time-varying heating to analyze the effect of periodic diurnal heating on a balanced vortex.

Most work on the TC diurnal cycle is devoted to documenting storm high cloudiness (Browner et al. 1977; Muramatsu 1983; Lajoie and Butterworth 1984; Steranka et al. 1984; Kossin 2002). A coherent diurnal signal is observed in the TC cirrus canopy, which propagates radially away from the storm center (Steranka et al. 1984; Dunion et al. 2014). This signal is consistent across ocean

---

---

[a] Current affiliation: The Weather Channel, Atlanta, Georgia.

Corresponding author: Erika L. Navarro, enavarr4@atmos.uw.edu

basins and is a function of the local solar time. Numerical modeling studies of the TC diurnal cycle show a wide range of results, with some studies showing a large impact in the developing stages (Sundqvist 1970; Hobgood 1986; Melhauser and Zhang 2014; Tang and Zhang 2016) and others showing impact during the mature stage (Hack and Schubert 1980; Tuleya and Kurihara 1981; Craig 1996; Tang and Zhang 2016). Currently, there is no consensus in the literature on the role of the diurnal cycle of radiation on TC structure and intensity.

NH2016 use an idealized, axisymmetric TC in a steady-state framework and demonstrate a clear signal in the temperature, wind, and latent heating tendency fields. This signal is statistically significant at the 95% level. Composite analysis of these fields at each hour of the day reveals a cycle in storm intensity that is a maximum in the early hours of the morning and lags a periodic response in latent heating by approximately 6 h. Average magnitudes of the diurnal signal in storm intensity are about $1 \, \text{m s}^{-1}$ near the radius of maximum wind (RMW). Inertia–buoyancy waves are observed in the upper troposphere and lower stratosphere, linked with positive temperature anomalies that arise in the TC outflow layer. NH2016 hypothesize that these periodic heat sources drive anomalous circulations in the upper and lower troposphere that drive the TC diurnal cycle.

The goal of this work is to test the NH2016 hypotheses by diagnosing the impact of periodic diurnal heating on a balanced vortex. The Sawyer–Eliassen equation has been used to compute the secondary flow induced by quasi-steady forcing in a balanced vortex (Schubert and Hack 1982; Shapiro and Willoughby 1982; Pendergrass and Willoughby 2009). Periodic, as compared to steady, forcing, however, requires a different formulation in which the governing equations are linearized about the mean vortex and describe periodic perturbations induced by periodic forcing on the mean vortex. The result is a second-order differential equation for the perturbation streamfunction, which is similar to the Sawyer–Eliassen equation except that the coefficients of the second derivatives are functions of the forcing frequency (Willoughby 2009). For low-frequency forcing, solutions project onto a slowly varying analog to the Sawyer–Eliassen equation; for high-frequency forcing, solutions project onto inertia–buoyancy waves.

The remainder of this paper is organized as follows. Description of the time-varying method, the vortex, and heating specification are given in section 2. Results are shown in section 3, and the sensitivity of the results to changes in the vortex intensity and the frequency of the forcing are described in section 4. Section 5 provides a discussion and the conclusions.

2. Methods

a. Model configuration

Using the method of Willoughby (2009), we solve for the perturbation mass flow streamfunction induced by periodic diurnal heating on a balanced vortex. A full derivation of this equation is given in Willoughby (2009); only the streamfunction equation and the solution method are described here.

Solving the governing system of equations for u and w and introducing a mass flow streamfunction ψ such that

$$r\rho u = \frac{\partial \psi}{\partial z}, \quad r\rho w = \frac{\partial \psi}{\partial r} \tag{1}$$

gives a second-order differential equation for the perturbation streamfunction (Willoughby 2009):

$$
(N^2 - \omega^2)\frac{\partial^2 \psi}{\partial r^2} - 2B\frac{\partial^2 \psi}{\partial r \partial z} + (I'^2 - \omega^2)\frac{\partial^2 \psi}{\partial z^2} - \left[\frac{(N^2 - \omega^2)}{R_{\theta\rho}} - \frac{B}{H_{\theta\rho}}\right]\frac{\partial \psi}{\partial r} -
$$
$$
\left[\frac{(I'^2 - \omega^2)}{H_{\theta\rho}} - \frac{B}{R_{\theta\rho}} - \frac{3\xi S}{r} + B\frac{\partial \gamma}{\partial z} - N^2\frac{\partial \gamma}{\partial r}\right]\frac{\partial \psi}{\partial z} = r\rho\left[\left(\frac{\partial}{\partial r} - \frac{1}{L_{\theta}}\right)Q - \left(\frac{\partial}{\partial z} - \frac{1}{H_{\theta}}\right)(\xi M - \gamma Q)\right], \tag{2}
$$

where

$$\frac{1}{R_{\theta\rho}} \equiv \frac{1}{r} + \frac{1}{\theta_0}\frac{\partial \theta_0}{\partial r} + \frac{1}{\rho}\frac{\partial \rho}{\partial r}, \tag{3a}$$

$$\frac{1}{H_{\theta\rho}} \equiv \frac{1}{\theta_0}\frac{\partial \theta_0}{\partial z} + \frac{1}{\rho}\frac{\partial \rho}{\partial z}, \tag{3b}$$

$$\frac{1}{L_{\theta}} \equiv \frac{1}{\theta_0}\frac{\partial \theta_0}{\partial r}, \quad \text{and} \tag{3c}$$

$$\frac{1}{H_{\theta}} \equiv \frac{1}{\theta_0}\frac{\partial \theta_0}{\partial z}. \tag{3d}$$

Here, $u(r, z, t)$ and $w(r, z, t)$ are the perturbation radial and vertical velocities, respectively. The perturbation azimuthal wind $v(r, z, t)$ is defined by

$$-i\omega v + \zeta u + Sw = M, \tag{4}$$

where perturbations are taken with respect to the mean vortex (Willoughby 2009). The mean-flow vertical

vorticity is given by $\zeta = \partial v_0/\partial r + v_0/r + f$, where v_0 is the mean vortex azimuthal wind and f is the Coriolis parameter, and the vertical wind shear is given by $S = \partial v_0/\partial z$. The M is the momentum forcing, which here is set equal to zero, and ω is the diabatic forcing frequency. The inertia parameter ξ is given by $2v_0/r + f$, and $I'^2 = (\zeta\xi)^2 - \gamma B$ is a modified local inertia frequency, where $\gamma = g^{-1}(v^2/r + fv)$ is the ratio of the mean-flow radial acceleration to gravity.[1] The radial and vertical gradients of the mean vortex buoyancy are $B = \partial b_0/\partial r$ and $N^2 = \partial b_0/\partial z$, where $b_0(r, z) = g\ln(\theta_0/273.16)$ is the mean-state buoyancy and θ_0 is the mean potential temperature. The radial buoyancy gradient has units of s^{-2} and N^2 is the square of the buoyancy frequency. The diabatic perturbation buoyancy is given by Q', where $Q' = gq/c_p\theta_0$, q is the diabatic heating rate, and c_p is the specific heat at constant pressure for dry air. The mean-state air density is given by $\rho = 1000\pi_0^{c_v/R}/R\theta_0$, where $\pi_0(r, z) = (p_0/1000)^{R/C_p}$ is the mean Exner function computed from the pressure, $p_0(r, z)$. The gas constant is given by R, and c_v is the specific heat of dry air at constant volume.

Equation (2) is similar to the classic Sawyer–Eliassen equation except that the coefficients of the second partial derivatives are functions of the forcing frequency and the character of the solution changes based on the sign of the coefficients. The discriminant of Eq. (2) defines the solution's behavior:

$$D^4 = (N^2 - \omega^2)(I'^2 - \omega^2) - B^2. \qquad (5)$$

When $D^4 > 0$, Eq. (2) is elliptic and the solution resembles the Sawyer–Eliassen solution. For $D^4 < 0$, Eq. (2) is hyperbolic and solutions project onto inertia–buoyancy waves. Since I'^2 is large in the storm core, and since the diurnal cycle is a low-frequency forcing (i.e., $\omega \ll I'$), we expect that solutions near the core of the storm will resemble the Sawyer–Eliassen solution. However, for solutions further from the center (i.e., $\omega \ge I'$) solutions will manifest as inertia–buoyancy waves.

Solutions are obtained using the Lindzen and Kuo (1969) algorithm for the specified forcing and initial vortex structure. The periodic forcing is sinusoidal and oscillates at a frequency of $\omega = 2\pi/\tau$, where $\tau = 24$ h. The domain extends from the surface to 30 km in the vertical and from the vortex center to 1500 km in the horizontal. Vertical and horizontal grid resolutions are 1.5 and 2 km, respectively. There is no axially symmetric flow into the surface, across the center of the vortex, or out of the top of the domain. A sponge layer is imposed at the domain

top to prevent reflection of inertia–buoyancy waves back down toward the surface. At the right edge of the domain $\partial\psi/\partial r = 0$, and flow is strictly horizontal. There is no friction. The vortex is defined from an idealized environmental sounding in which the temperature decreases from 300 K at the surface to 200 K at the tropopause (15 km) and is isothermal at 200 K in the stratosphere.

The mean vortex is similar to the "idealized vortex" described in Pendergrass and Willoughby (2009) and Willoughby (2009), except the location of the RMW and the vortex intensity have been modified for comparison with the numerical simulation used in this study. Winds decrease linearly with height from the surface to the top of the vortex at 18.5 km (Fig. 1). Maximum values of $37 \, \mathrm{m\,s}^{-1}$ are specified at the surface. The RMW tilts outward with height from a radius of 53 km at the surface to a radius of 70 km at 18.5-km height, indicating the top of the vortex. Inside the RMW winds increase linearly with radius; outside the RMW, winds decrease exponentially with an e-folding distance of 300 km. The transition zone in the region of the RMW is 20 km wide and is a weighted sum of the inner and outer wind profiles (Willoughby et al. 2006).

Figure 2 shows the discriminant of Eq. (2), which defines the boundary between elliptic and hyperbolic solution domains. The zero contour gradually slopes downward from the upper troposphere to the surface with increasing radius from storm center. Positive values fill the core of the storm. They are largest between 0 and 100 km in radius and up to 19 km in height. This reflects the large gradient of local inertial frequency in this region and indicates elliptic solutions similar to the Sawyer–Eliassen solution. Above 19 km, and for radii beyond 350 km at the surface, values of the discriminant are negative, which indicates that solutions in this region will manifest as inertia–buoyancy waves.

b. Heating distributions

The hypotheses introduced in NH2016 are derived from a simulation produced in an axisymmetric configuration of Cloud Model 1 (CM1), which is a non-hydrostatic cloud model that simulates the effects of shortwave and longwave radiation (Bryan and Rotunno 2009b). A full description of the model initialization and physics is given in section 2a of NH2016; here, we will only review the proposed hypotheses. Figures 3a,b show the CM1 heating distributions, which comprise two distinct, periodic heat sources. These heating distributions represent composite anomalies from the time–mean storm at the indicated times. At 0300 local time (LT), a maximum in the composite latent heating tendency anomaly occurs in the lower troposphere near the

---

[1] The I' and γ terms arise as a result of the derivation in height instead of pressure coordinates.
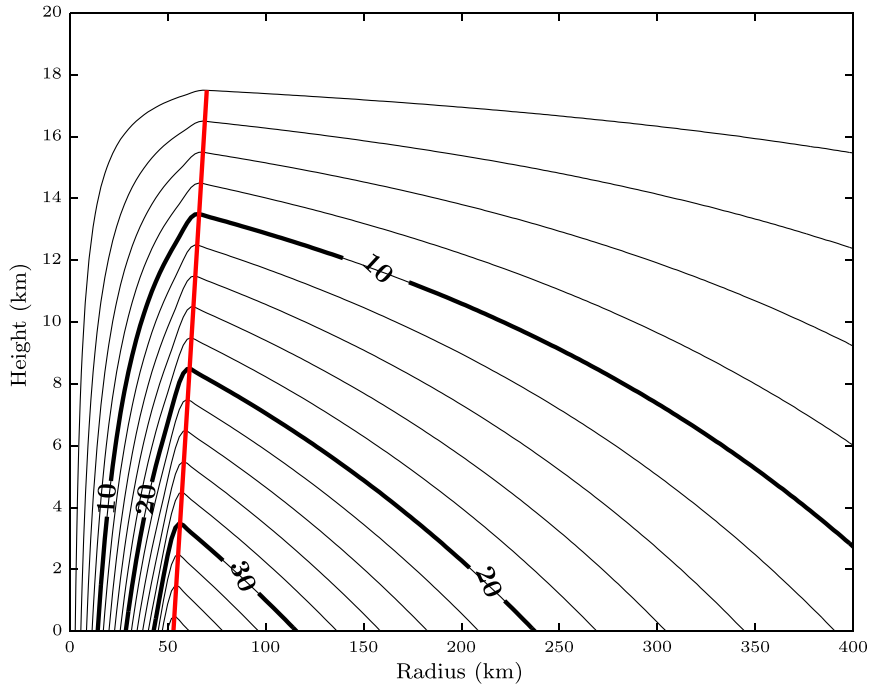
FIG. 1. The mean vortex azimuthal wind (m s^{-1}). The solid red line indicates the location of the RMW.

RMW, whose mean location is at a radius 53 km (Fig. 3a). Values of the latent heating tendency anomalies are 1.2 K h^{-1} near a radius of 50 km and from 2 to 8 km in height. This heating is associated with a layer of radial inflow extending from 50 to 400 km in radius and exhibiting an average magnitude of 1 m s^{-1}. Anomalous upward motion is present in the region of peak heating, with values near 5 cm s^{-1}. The anomalous
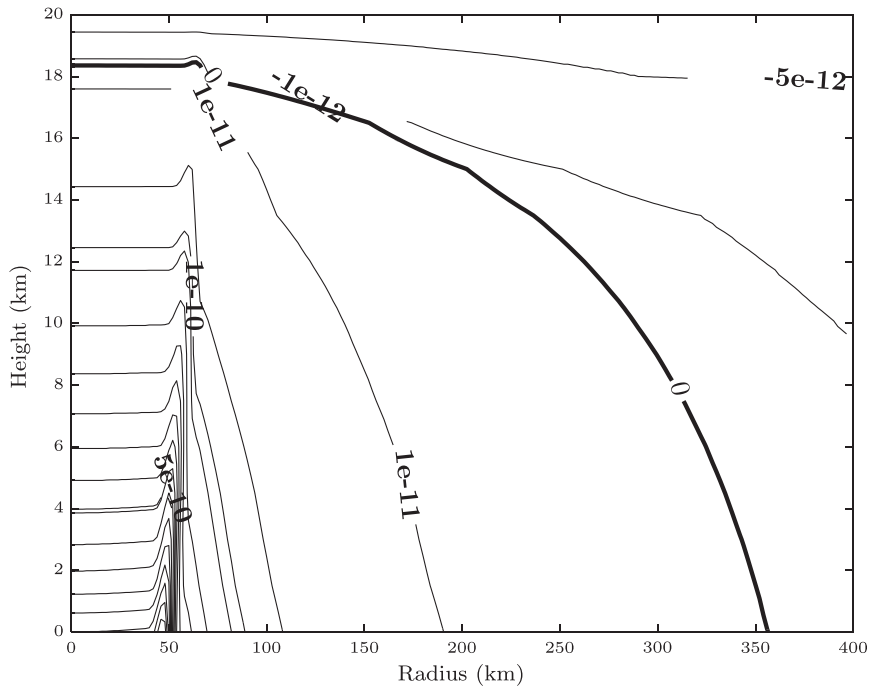

FIG. 2. The discriminant (s^{-4}) for the initial vortex shown in Fig. 1.

Latent Heating Tendency, 3:00 LT
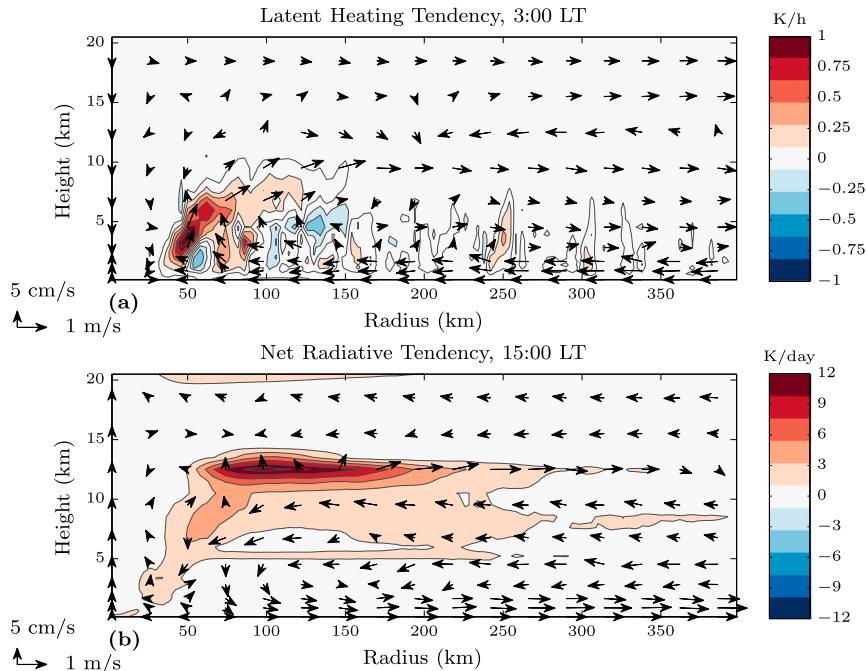

Net Radiative Tendency, 15:00 LT

FIG. 3. The hypotheses presented in NH2016, showing (a) the composite latent heating tendency anomaly at 0300 LT and (b) the composite net radiative tendency anomaly at 1500 LT for the idealized, steady-state CM1 simulation. The radial–vertical wind vectors at each time are plotted for reference. The maximum vertical velocity of $10 \, \text{cm s}^{-1}$ is not well represented by the reference vector. These figures have been reproduced from NH2016.

flow turns outward at 10-km height and exits the core of the storm at this level. At 1500 LT, radiative heating warms the upper troposphere near the level of the TC outflow (Fig. 3b). This anomalous heating is a maximum at 12.5-km height and exhibits a magnitude of $12 \, \text{K day}^{-1}$. Anomalous upward motion occurs near the center of heating, with anomalous radial inflow near $1 \, \text{m s}^{-1}$ below the region of heating. At the level of heating, anomalous radial outflow occurs. In both cases, heating and the associated circulations are periodic with respect to the diurnal cycle.

Figure 4 shows the idealized versions of these two heat sources for use in the Willoughby (2009) time-varying model. We will refer to solutions from this method as the "diagnostic solutions." The heating field described in NH2016 is partitioned into two separate configurations to determine the impact of periodic diurnal heating in each layer.[2] The maximum amplitude of the heating occurs at $t = 0$, and the minimum at $t = 12 \, \text{h}$. Unless otherwise noted, all solutions from the diagnostic model are shown at a time of $t = 0$. In the diagnostic model, the

CM1 latent heating tendency is represented by a diabatic low-level heating maximum with a center at 53 km in radius and 5 km above the surface (Fig. 4a). This heating has a width of 40 km and a height of 7 km. The maximum magnitude of this heating is $1 \, \text{K h}^{-1}$, which is consistent with the CM1 solutions. This heating is well inside the boundary defined by the discriminant, which suggests elliptic solutions. The CM1 radiative forcing is represented by a heating maximum placed in the upper troposphere at a height of 10.5 km (Fig. 4b). The level of upper-level heating in the diagnostic model is lower than in the CM1 simulation; however, it occurs at a similar height relative to the mean vortex. The center of this heating is at 100-km radius, and it exhibits a width of 75 km in the radial direction. The maximum magnitude of the upper-level heating is $12 \, \text{K day}^{-1}$. The heating is in close proximity to the boundary given by the discriminant and suggests that solutions may involve a combination of elliptic and hyperbolic solution types.

3. Results

a. Lower-tropospheric forcing

Periodic forcing near the storm core induces a perturbation wind response in the lower troposphere

---

[2] Since the diagnostic model is linear, the induced response from both idealized heat sources may be added together to simulate the full CM1 response.
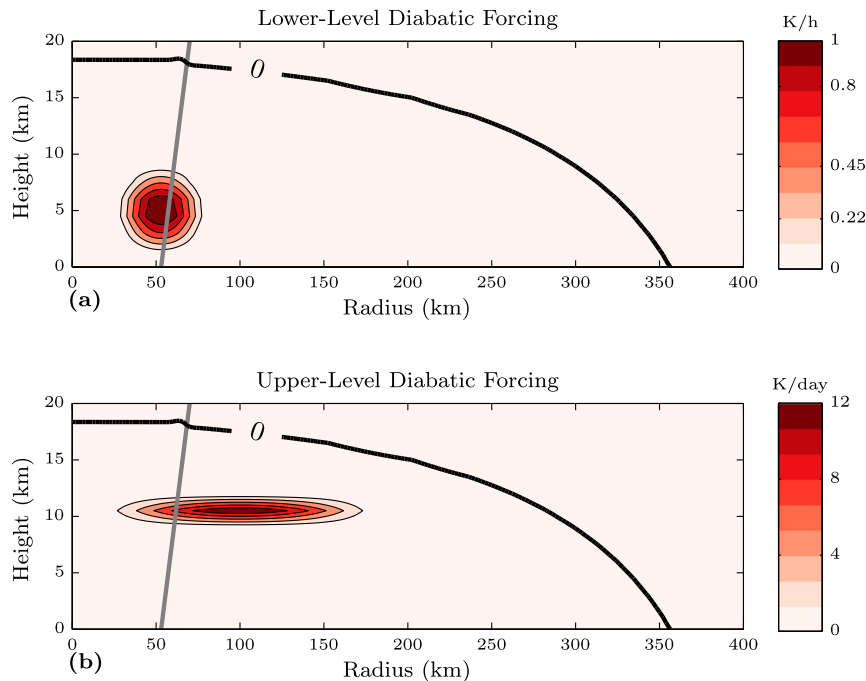
FIG. 4. The periodic diurnal heat sources used in the Willoughby (2009) model for (a) the low-level forcing and (b) the upper-level forcing. The solid gray line indicates the mean location of the RMW. The zero contour of the discriminant is plotted for reference.

(Fig. 5a). Radial inflow occurs near the surface from the RMW to 400 km and extends up to 4-km height. Magnitudes of radial inflow are largest near the RMW, with values of $-0.4\,\mathrm{m\,s}^{-1}$ from 50 to 100 km, and decrease outward to $-0.1\,\mathrm{m\,s}^{-1}$ in the storm environment. Radial outflow occurs from the RMW to a radius 300 km and extends vertically from 6 to 12 km. Magnitudes of radial outflow are $0.4\,\mathrm{m\,s}^{-1}$ near the RMW and gradually decrease to $0.1\,\mathrm{m\,s}^{-1}$ in the exterior storm environment. Weak values of radial inflow of $-0.1\,\mathrm{m\,s}^{-1}$ are observed inside the RMW from 5–10-km height, indicating divergence at this level. Upward motion occurs in the region of heating at the RMW (Fig. 5b), consistent with the divergence in the midtroposphere. A maximum value in vertical velocity of $0.06\,\mathrm{m\,s}^{-1}$ is observed in the region of the RMW at 5-km height. The structure of the radial and vertical motion suggests an overturning circulation in the lower troposphere, resembling what one expects from the classic Sawyer–Eliassen solution. This balanced response in the diagnostic model is expected based on the positive values of the discriminant [Eq. (5)]. The corresponding CM1 radial wind indicates a similar structure to the diagnostic solution (Fig. 5c). Radial inflow occurs near the surface from 100 to 400 km, with a maximum magnitude of $-0.8\,\mathrm{m\,s}^{-1}$. Radial outflow is indicated from 100 to 400 km in radius from 2- to 6-km height and again from 100 to 400 km in radius and from 8 to 12 km in height.

Alternating positive and negative values occur throughout the troposphere and into the lower stratosphere, suggesting a wave response. Positive values of vertical velocity occur at the RMW (Fig. 5d). Magnitudes in vertical velocity near $0.07\,\mathrm{m\,s}^{-1}$ occur from 40 to 100 km in radius and extend from just above the surface to near 12 km in height, similar to the diagnostic solution. While the CM1 solution exhibits finer-scale structures, the overturning of the winds resembles a Sawyer–Eliassen-like response and suggests a correspondence to the diagnostic solution. The wavelike features in the upper troposphere of the CM1 solution reflect the influence of the upper-level heating and are discussed below.

The perturbation azimuthal wind for the diagnostic solution shows a low-level maximum at the RMW (Fig. 6a). This maximum in the perturbation azimuthal wind lags the maximum in the perturbation streamfunction by 6 h. Perturbation amplitudes of $2.5\,\mathrm{m\,s}^{-1}$ are indicated at the surface near a radius of 50 km and extend upward to 4 km. Positive perturbations extend radially outwards to 100 km and upward to 8 km, tilting inward with height. Negative values are indicated inside the eye from 0 to 50 km, as well as outside the RMW in the midtroposphere from 6 to 10 km in height and 50 to 150 km in radius. The CM1 composite azimuthal wind anomalies shows a weaker, similar structure in the low levels (Fig. 6b). The model simulates this response
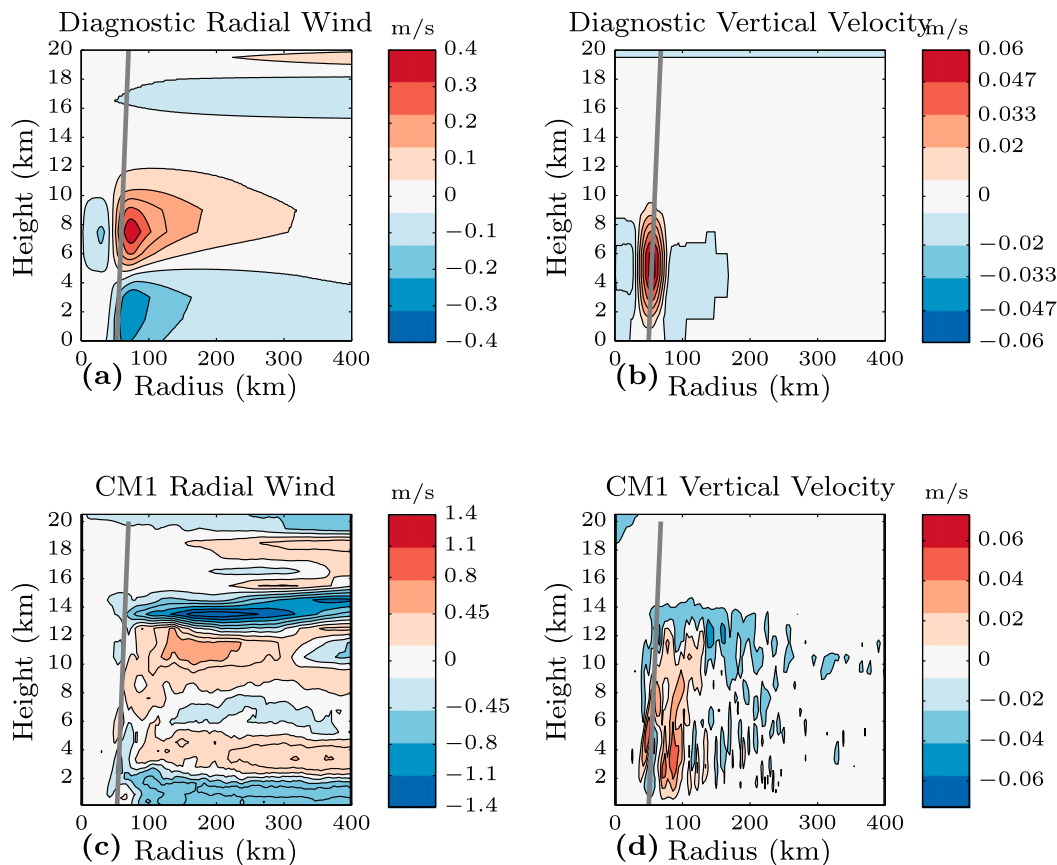
FIG. 5. The diagnostic perturbation (a) radial and (b) vertical velocity (m s^{-1}) for the low-level forcing in Fig. 4a and the CM1 composite anomalies of the (c) radial and (d) vertical velocity at 0100 LT. The solid gray line indicates the mean location of the RMW. The ranges of the color bars differ between the diagnostic and CM1 solutions.

6 h after the maximum in anomalous latent heating tendency, which occurs at 0100 LT. A low-level maximum of 0.75 m s^{-1} is indicated from 50 to 100 km in radius and up to 6 km in height. This anomaly extends through the TC boundary layer from 50 to 400 km in radius and up to 2 km in height. Negative values of up to 0.5 m s^{-1} are demonstrated both inside the eye and throughout the mid- to upper troposphere. Weak positive anomalies are indicated inside the eye from 8- to 10-km height, similar to the diagnostic solution. For both models, these results suggest the low-level azimuthal wind accelerates in response to low-level periodic forcing. Azimuthal wind maxima just outside the RMW also indicate a broadening of this region and a possible increase in storm size.

b. Upper-level forcing

Periodic diurnal heating near the top of the storm produces a localized overturning circulation (Fig. 7a). Air moves inward toward the base of the heat source from 6- to 10-km height and outward above the region of

heating from 10- to 14-km height. Maximum absolute values of radial velocity are 0.5 m s^{-1} for positive and negative values. In the region of heating, upward motion occurs (Fig. 7b). Maximum values of vertical velocity are 0.03 m s^{-1} at a radius of 100 km and a height of 10.5 km. For radii of 300–400 km, alternating positive and negative anomalies occur from the surface up to the lower stratosphere; this suggests an inertia–buoyancy wave response in the exterior storm environment. This response is consistent with the negative values of the discriminant in this region. The CM1 radial inflow indicates similar structures (Fig. 7c). Radial inflow occurs at the base of the heating from 100 to 250 km in radius and from 10 to 12 km in height, as well as from 250 to 400 km in radius and near 13-km height. Radial outflow occurs from 100 to 400 km in radius and from 10- to 15-km height. Maximum magnitudes of radial velocity approach 1.5 m s^{-1} for positive values and minimum magnitudes approach −1.0 m s^{-1} for negative values. Alternating negative and positive anomalies are observed at large radii from the surface to the lower stratosphere, indicating an inertia–buoyancy
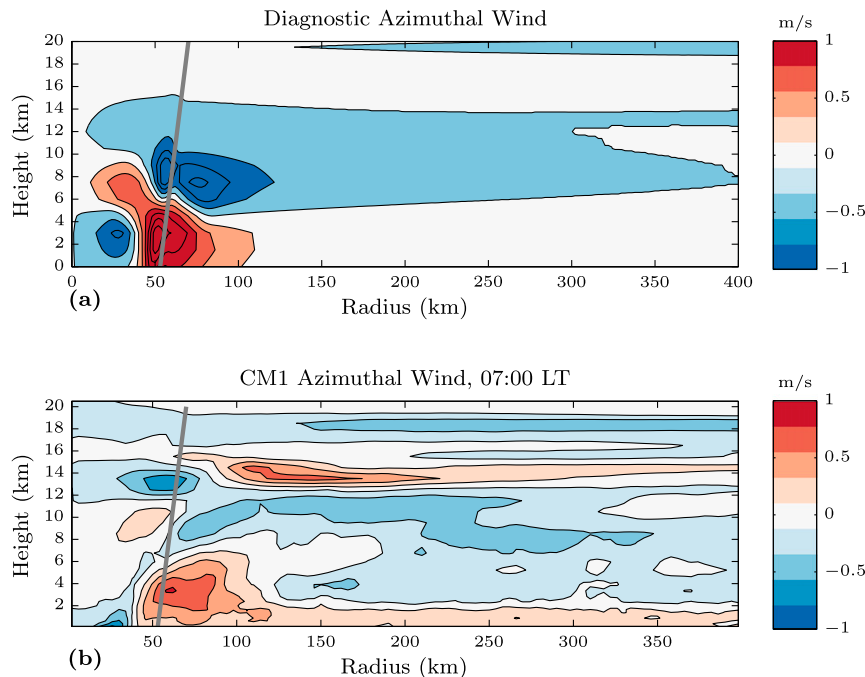
FIG. 6. (a) The diagnostic perturbation azimuthal wind (m s^{-1}) for the low-level forcing and (b) the CM1 composite azimuthal wind anomaly (m s^{-1}) at 0700 LT. The solid gray line indicates the mean location of the RMW. The diagnostic perturbation azimuthal wind lags the maximum in perturbation streamfunction by 6 h.

wave response. Upward motion occurs in the upper troposphere from 100- to 200-km radius and 10 to 14 km in height, similar to the diagnostic solution (Fig. 7d). The CM1 solution shows a close correspondence to the diagnostic solution, suggesting a localized, balanced response in the region of heating and an inertia–buoyancy wave response in the exterior storm environment. The radial and vertical motion occurring in the lower troposphere is dominated by the low-level heating response.

The perturbation azimuthal wind for the upper-level forcing exhibits a symmetric "quadrupole" structure (Fig. 8a). This maximum in perturbation azimuthal wind lags the maximum in perturbation streamfunction by 6 h. This response is mainly confined to the mid- to upper troposphere. Positive values occur from 50 to 400 km in radius and 6 to 10 km in height, with negative values from 50 to 400 km in radius and 10 to 14 km in height. Inside the RMW the sign changes, with negative values indicated from 0 to 50 km in radius and 5 to 10 km in height, and positive values from near 20 to 50 km in radius and from 10 to 12 km height. Maximum magnitudes of these perturbations are 0.25 m s^{-1} for both positive and negative perturbations. Comparing this result to the corresponding CM1 azimuthal wind anomaly shows a similar structure in the upper troposphere (Fig. 8b). The

model simulates this response 6 h after the maximum in shortwave heating tendency, which occurs at 1300 LT.[3] Positive values are indicated from 50 to 250 km in radius and 6 to 12 km in height, and negative values are present from 50 to 400 km in radius and 12- to 16-km height. Inside the RMW, negative values occur from 0 to 50 km in radius and 2 to 10 km in height and positive values from 25 to 50 km in radius and 12 to 15 km in height. There is a close correspondence between the diagnostic solution and the CM1 results, which suggests that upper-level periodic heating is driving the CM1 azimuthal wind response in this region. In the lower troposphere, negative anomalies near the RMW and throughout the TC boundary layer correspond to the cooling phase of the CM1 low-level forcing (Fig. 6b).

4. Sensitivity

Figure 9 shows the discriminant boundary for different values of the mean vortex intensity used in the diagnostic model. Since N^2 and B in Eq. (5) are determined by the temperature profile, the sensitivity of

---

[3] The maximum in the shortwave heating tendency lags the maximum in the incoming solar flux by 1 h.
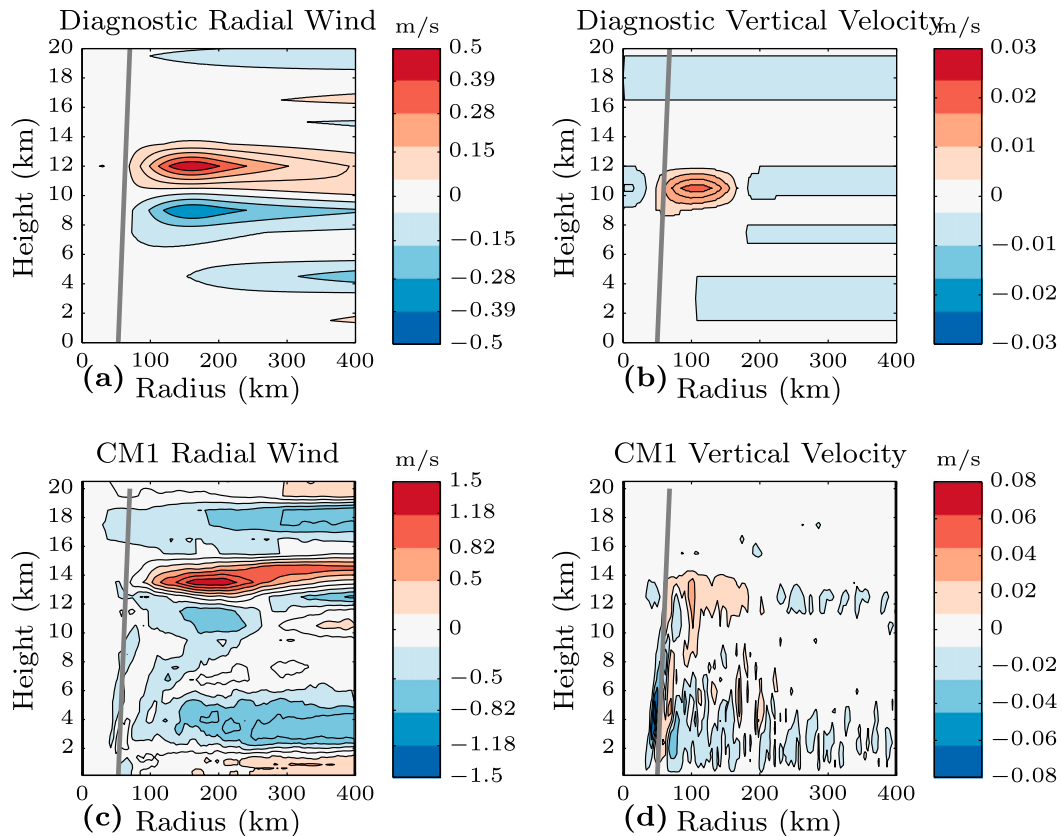
FIG. 7. The diagnostic perturbation (a) radial and (b) vertical velocity (m s^{-1}) for the upper-level forcing in Fig. 4b, and the CM1 composite anomalies of the (c) radial and (d) vertical velocity at 1300 LT. The solid gray line indicates the mean location of the RMW. The ranges of the color bars differ between the diagnostic and CM1 solutions.

the diagnostic solutions can be easily investigated by modifying either ω or I' through the mean vortex intensity. For an initial vortex of $5 \, \mathrm{m \, s^{-1}}$, the discriminant boundary extends from near 16-km height down to 150 km at the surface, remaining near the core of the storm. As the intensity of the mean vortex increases, the discriminant boundary expands upward and outward, with values near the surface extending from 150 km in radius to 375 km for an initial vortex intensity of $60 \, \mathrm{m \, s^{-1}}$. In the vertical, the discriminant boundary expands from 16 to 19 km and gradually slopes downward and outward as the mean vortex intensity increases. This suggests that all storms will exhibit elliptic solutions inside of 150 km but will exhibit hyperbolic solutions in the outer storm environment based on the vortex intensity. Higher-perturbation azimuthal winds occur for stronger vortices, suggesting that the magnitude of the diurnal signal may vary throughout the lifetime of the storm (not shown).

Figure 10 demonstrates results from two experiments in which the length of the diurnal period is modified in

both the diagnostic framework and in CM1. The CM1 simulations with a modified diurnal period are the same as NH2016, except that local solar time and the hour angle (i.e., the difference between local solar time and solar noon) are modified to increase or decrease the length of the diurnal period.[4] For a diurnal period of 6 h, wave solutions are indicated in response to upper-level heating throughout the domain (Fig. 10a). Magnitudes are near $0.24 \, \mathrm{m \, s^{-1}}$ from 6- to 20-km height for positive and negative perturbations. For a period of 72 h, the model simulates a balanced, more symmetric response (Fig. 10b). Positive values are indicated below the heat source from 50 to 300 km in radius and from 5- to 10-km height and negative values occur inside the RMW from 0 to 50 km. Above the heating, negative perturbations are indicated from 50 to 400 km in radius and from 12- to 15-km height, and positive values are indicated inside the RMW

---

[4] These changes only affect the radiation scheme, such that the rotation rate of Earth and the Coriolis parameter remain fixed.
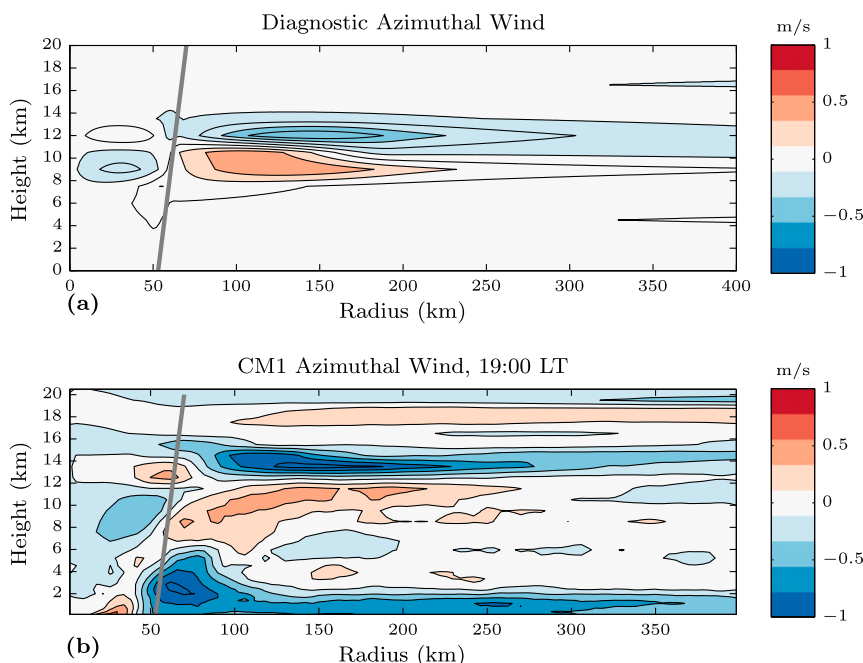
FIG. 8. (a) The diagnostic perturbation azimuthal wind (m s^{-1}) for the upper-level forcing and (b) the CM1 composite azimuthal wind anomaly at 1900 LT. The solid gray line indicates the mean location of the RMW. The diagnostic perturbation azimuthal wind lags the maximum in perturbation streamfunction by 6 h.

from 0- to 50-km radius and 11- to 13-km height. The magnitude of these perturbations is 1.3 m s^{-1} for a period of 72 h, which is 5 times larger than the solutions for a 6-h diurnal period.

The corresponding CM1 azimuthal wind anomalies for upper-level forcing for a 6-h diurnal period also show a wavelike response throughout the domain (Fig. 10c).[5] Alternating positive and negative anomalies occur throughout the upper troposphere and lower stratosphere, with absolute values near 0.2 m s^{-1}. In the lower troposphere, the azimuthal wind anomalies are mostly negative, with magnitudes near -0.1 m s^{-1}. These results are similar to the diagnostic solution, which suggest an inertia–buoyancy wave response to upper-level periodic heating. The composite azimuthal wind anomalies for the 72-h diurnal period show a well-defined upper- and lower-tropospheric response (Fig. 10d). Positive azimuthal wind anomalies are indicated near 10-km height and from 50 to 300 km in radius, which extend down to the surface near the RMW. Negative azimuthal wind anomalies occur from 50 to 400 km in radius and from 10

to 14 km in height and demonstrate the same symmetric quadrupole pattern in the upper troposphere as the diagnostic solution. The magnitude of the upper-level azimuthal wind anomalies are near 0.5^{-1}, which is about half of the value in the diagnostic solutions. At the surface, positive azimuthal wind anomalies of 2.5 m s^{-1} are simulated inside the RMW, indicating storm intensification. This amplification of the azimuthal wind response in the low levels suggests a possible feedback from the heating in the lower levels.

5. Discussion

Here, a modified Sawyer–Eliassen equation for time-varying forcing is applied to diagnose the role of periodic diurnal heating on a balanced vortex. Following the work of NH2016, two regions of periodic diurnal heating are analyzed: 1) upper-tropospheric heating by absorption of solar radiation near the TC outflow layer and 2) lower-tropospheric heating due to latent heat release by convection. These distributions are considered separately to determine their relative impact on the vortex circulation. Time-varying heating requires a specific formulation where the governing equations are linearized about the mean state (Willoughby 2009); the result is an equation for the perturbation streamfunction, where the solutions

---

[5] Since the time scale for geostrophic adjustment in CM1 is approximately 9 h, which is greater than the modified diurnal period for this experiment, we utilize a lag of 3 h here to analyze the perturbation azimuthal wind response.
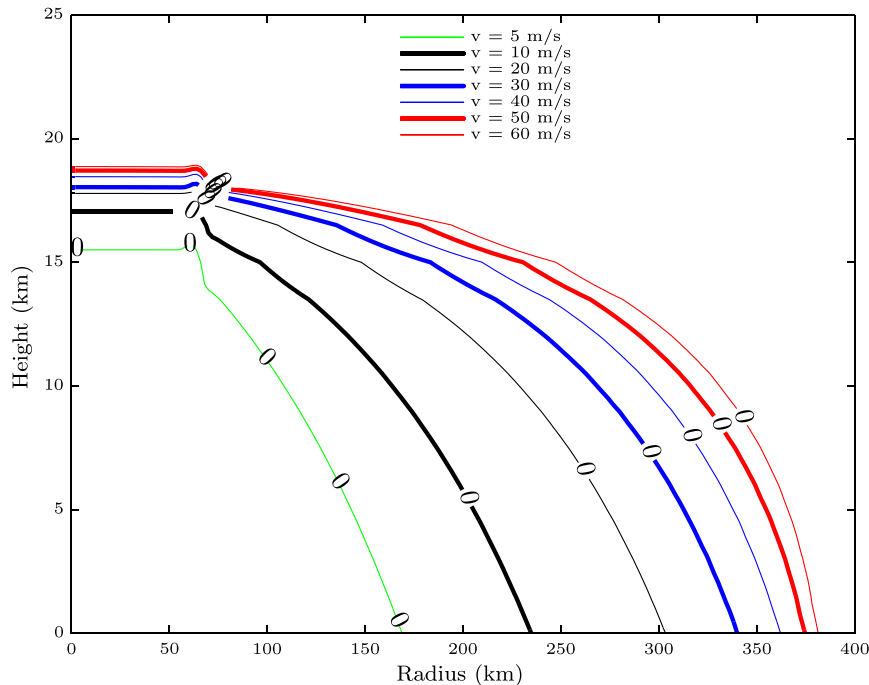
FIG. 9. The discriminant (s^{-4}) of the diagnostic solution for different values of the mean vortex intensity: $v = 5$ (green), 10 (black), 20 (gray), 30 (thick blue), 40 (thin blue), 50 (thick red), and 60 (thin red) m s^{-1}. The period of forcing is fixed at 24 h.

describe periodic perturbations on the mean vortex. Results for low-frequency forcing in the storm core approach the classic Sawyer–Eliassen solution, while solutions further in the exterior environment project onto inertia–buoyancy waves.

For both upper-level and lower-level periodic forcing, comparison between the diagnostic solution and the CM1 numerical simulation in NH2016 demonstrates a similar response. Periodic diurnal heating in the storm core drives an overturning response throughout the lower to midtroposphere, which is a slowly varying analog to the Sawyer–Eliassen secondary circulation. This is associated with an acceleration of the low-level azimuthal wind 6 h after the maximum in heating. Periodic heating in the upper troposphere induces a local overturning response in the region of heating, which manifests as inertia–buoyancy waves in the storm environment. In both cases, the CM1 composite azimuthal wind anomalies exhibit a similar response, with an overturning circulation indicated in the lower levels following a maximum in anomalous latent heating tendency and a local, overturning circulation in the upper troposphere following a maximum in upper-level radiative heating. This suggests that diurnal periodic heating is driving the CM1 response in the wind field, as well as the storm intensity. Partitioning of the CM1 heating field into two parts

demonstrates that low-level periodic heating dominates the lower-tropospheric response, while the response to upper-level forcing is mainly confined to the upper troposphere.

The similarity of the structure between the diagnostic solution and the CM1 diurnal cycle suggests that the axisymmetric TC diurnal cycle in CM1 is the combined response from two periodic heat sources. These heat sources are out of phase with each other, indicating that upper-level radiative heating may be indirectly related to the low-level latent heat release. Since the diagnostic model is linear, the solutions for the upper-level and lower-level heating can be added together to calculate the combined response. However, since the Willoughby (2009) method requires prior knowledge of the heating field, and does not explicitly solve for the effects of radiation or microphysics, we are unable to investigate the dynamic relationship between these two features in this model. Analysis of the dynamic coupling between the upper-level and lower-level response in a numerical simulation is suggested as one possible avenue of future work.

These results depend on the chosen initial vortex, so that factors such as the mean vortex azimuthal wind, the location of the RMW, and the decay length of the outer wind profile all contribute to the location of the discriminant boundary and, therefore, the impact
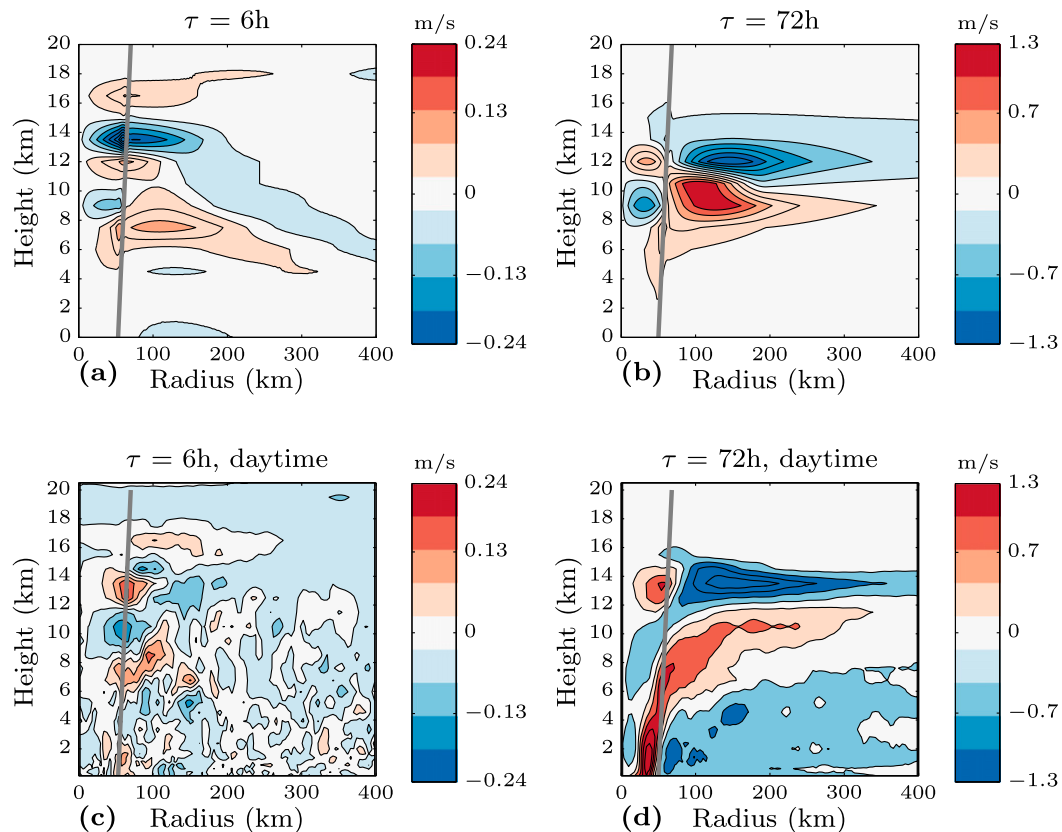
FIG. 10. The perturbation azimuthal wind (m s^{-1}) for upper-level heating for (a),(b) the diagnostic solution and (c),(d) CM1. (left) A diurnal period of 6 h and (right) a period of 72 h. The solid gray line indicates the mean location of the RMW in each simulation.

of periodic diurnal heating. The sensitivity of these solutions with respect to the period of the forcing as well as the mean vortex intensity demonstrates that the structure and magnitude of the TC diurnal cycle exhibits large variance. Short diurnal periods project onto inertia–buoyancy waves, which radiate energy away from the region of heating, while long diurnal periods exhibit a more balanced solution that has a larger impact on the storm intensity. This implies that the magnitude of the TC diurnal signal is dependent on the length of the heating phase, with longer periods producing a stronger perturbation wind response. For a fixed period of 24 h, weaker initial vortices produce weaker azimuthal wind perturbations, with the magnitude of the diurnal signal scaling linearly with the intensity of the vortex. Since the period of the diurnal signal does not vary in nature, Eq. (5) demonstrates that as the inertial frequency changes, the response to periodic heating will change, producing steadier or more wavelike solutions based on the relationship between ω and I. This suggests that stronger storms exhibit a larger diurnal signal and that the TC diurnal cycle may vary based on the mean state of the vortex.

This work does not consider variations in static stability or buoyancy, which may also affect the strength and structure of the diurnal signal. However, given the close correspondence of the results of the diagnostic model to the CM1 response, we expect the influence to be minor. Since the heating fields in the axisymmetric model are azimuthally averaged, the magnitude of the diurnal signal may be overestimated, which affects the strength of the induced circulations. Further work evaluating both the role of asymmetries in the TC outflow layer as well as the relationship between the microphysics and the radiative heating rates are suggested as two possible avenues of future study.

REFERENCES

Browner, S. P., W. L. Woodley, and C. G. Griffith, 1977: Diurnal oscillation of the area of cloudiness associated with tropical storms. *Mon. Wea. Rev.*, **105**, 856–864, doi:10.1175/1520-0493(1977)105<0856:DOOTAO>2.0.CO;2.

Bryan, G. H., and R. Rotunno, 2009b: The maximum intensity of tropical cyclones in axisymmetric numerical model simulations. *Mon. Wea. Rev.*, **137**, 1770–1789, doi:10.1175/2008MWR2709.1.

Craig, G. C., 1996: Numerical experiments on radiation and tropical cyclones. *Quart. J. Roy. Meteor. Soc.*, **122**, 415–422, doi:10.1002/qj.49712253006.

Dunion, J. P., C. D. Thorncroft, and C. S. Velden, 2014: The tropical cyclone diurnal cycle of mature hurricanes. *Mon. Wea. Rev.*, **142**, 3900–3919, doi:10.1175/MWR-D-13-00191.1.

Hack, J. J., and W. H. Schubert, 1980: The role of convective-scale processes in tropical cyclone development. Colorado State University Dept. of Atmospheric Science Rep. 330, 206 pp., https://dspace.library.colostate.edu/handle/10217/203.

Hobgood, J., 1986: A possible mechanism for the diurnal oscillations of tropical cyclones. *J. Atmos. Sci.*, **43**, 2901–2922, doi:10.1175/1520-0469(1986)043<2901:APMFTD>2.0.CO;2.

Kossin, J., 2002: Daily hurricane variability inferred from GOES infrared imagery. *Mon. Wea. Rev.*, **130**, 2260–2270, doi:10.1175/1520-0493(2002)130<2260:DHVIFG>2.0.CO;2.

Lajoie, F., and I. Butterworth, 1984: Oscillation of high-level cirrus and heavy precipitation around Australian region tropical cyclones. *Mon. Wea. Rev.*, **112**, 535–544, doi:10.1175/1520-0493(1984)112<0535:OOHLCA>2.0.CO;2.

Lindzen, R. S., and H. L. Kuo, 1969: A reliable method for the numerical integration of a large class of ordinary and partial differential equations. *Mon. Wea. Rev.*, **97**, 732–734, doi:10.1175/1520-0493(1969)097<0732:ARMFTN>2.3.CO;2.

Melhauser, C., and F. Zhang, 2014: Diurnal radiation cycle impact on the pre-genesis environment of Hurricane Karl (2010). *J. Atmos. Sci.*, **71**, 1241–1259, doi:10.1175/JAS-D-13-0116.1.

Muramatsu, T., 1983: Diurnal variations of satellite-measured TBB areal distribution and eye diameter of nature typhoons. *J. Meteor. Soc. Japan*, **61**, 77–90, doi:10.2151/jmsj1965.61.1_77.

Navarro, E. L., and G. J. Hakim, 2016: Idealized numerical modeling of the diurnal cycle of tropical cyclones. *J. Atmos. Sci.*, **73**, 4189–4201, doi:10.1175/JAS-D-15-0349.1.

Pendergrass, A. G., and H. E. Willoughby, 2009: Diabatically induced secondary flows in tropical cyclones. Part I: Quasi-steady forcing. *Mon. Wea. Rev.*, **137**, 805–821, doi:10.1175/2008MWR2657.1.

Schubert, W., and J. Hack, 1982: Inertial stability and tropical cyclone development. *J. Atmos. Sci.*, **39**, 1687–1697, doi:10.1175/1520-0469(1982)039<1687:ISATCD>2.0.CO;2.

Shapiro, L., and H. E. Willoughby, 1982: The response of balanced hurricanes to local sources of heat and momentum. *J. Atmos. Sci.*, **39**, 378–394, doi:10.1175/1520-0469(1982)039<0378:TROBHT>2.0.CO;2.

Steranka, J., E. Rodgers, and R. Gentry, 1984: The role of equivalent blackbody temperature in the study of Atlantic Ocean tropical cyclones. *Mon. Wea. Rev.*, **112**, 2338–2344, doi:10.1175/1520-0493(1984)112<2338:TDVOAO>2.0.CO;2.

Sundqvist, H., 1970: Numerical simulation of the development of tropical cyclones with a ten-level model. Part II. *Tellus*, **22**, 504–510, doi:10.1111/j.2153-3490.1970.tb00516.x.

Tang, X., and F. Zhang, 2016: Impacts of the diurnal radiation cycle on the formation, intensity, and structure of Hurricane Edouard (2014). *J. Atmos. Sci.*, **73**, 2871–2892, doi:10.1175/JAS-D-15-0283.1.

Tuleya, R. E., and Y. Kurihara, 1981: A numerical study on the effects of environmental flow on tropical storm genesis. *Mon. Wea. Rev.*, **109**, 2487–2506, doi:10.1175/1520-0493(1981)109<2487:ANSOTE>2.0.CO;2.

Willoughby, H. E., 2009: Diabatically induced secondary flows in tropical cyclones. Part II: Periodic forcing. *Mon. Wea. Rev.*, **137**, 822–835, doi:10.1175/2008MWR2658.1.

——, R. W. R. Darling, and M. E. Rahn, 2006: Parametric representation of the primary hurricane vortex. Part II: A new family of sectionally continuous profiles. *Mon. Wea. Rev.*, **134**, 1102–1120, doi:10.1175/MWR3106.1.